Colloids and Surfaces B: Biointerfaces 112 (2013) 219–228

Contents lists available at ScienceDirect

Colloids and Surfaces B: Biointerfaces

journal homepage: www.elsevier.com/locate/colsurfb

Recombinant bacteriophages as gold binding bio-templates

Nuriye Korkmaz*

Convergence Bioscience Group, Nanomedicine Team, Korea Institute of Science and Technology, Europe Forschungsgesellschaft mbH, Campus E 71, D-66123 Saarbrücken, Germany

ARTICLE INFO

Article history:
Received 8 March 2013
Received in revised form 3 July 2013
Accepted 30 July 2013
Available online xxx

Keywords:
Bacteriophage
Genetic engineering
Gold
Nanoparticle
Metallization
SEM

ABSTRACT

Bacteriophages are nano-sized virion particles infecting bacteria. In this study, it is shown that metal binding properties of filamentous fd-bacteriophages can be enhanced by genetic engineering. Quartz crystal microbalance (QCM) analyses, UV–vis absorption spectra measurements and scanning electron microscopy (SEM) imaging revealed that expression of MMM short amino acid sequence on major coat protein p8 facilitates recombinant MMM-phage binding to Au surfaces and nanoparticles (NPs) via gold–sulfur (Au—S) interaction. Electroless deposition of Au particles on phage assemblies was investigated upon chemical reduction reaction with $NaBH_4$ at different $HAuCl_4$ precursor concentrations. Energy dispersive X-ray spectroscopy (EDX) measurements confirmed the presence of Au on both AuNP decorated and chemically metallized phage structures. Further studies on patterning and controlled immobilization of recombinant bacteriophages on specific surfaces may contribute to bio-templated nanowire development field and biosensor application studies.

1. Introduction

Bottom-up manufacturing is an advantageous method in order to obtain nano-sized electronic device components in a simpler and more economical manner [1]. Top-down manufacturing, on the other hand, can bring some device integration and configuration problems [2,3]. Various bionano-structures such as DNA [4], virus particles [5] and bacterial surface layer proteins (S-layers) [6] have been used as building blocks for bottom-up production technology. For example, nucleic acid filaments were chemically modified and applied in nanoelectronics [7], catalytic research [8] and biosensor development [9] studies. Due to the ease of amplification, isolation and genetic modification of bacteriophages, different members of filamentous phages have been applied in inorganic bio-templating studies [10].

The filamentous fd-phage (~1–2 μm long, ~6 nm thick) consists of coat proteins surrounding a circular single stranded DNA (ssDNA) [11]. Major coat protein p8 (~2700–3000 copies) line up along the ssDNA [12]. Minor coat proteins p3 and p6 (5 copies) are found at one end and p7 and p9 (3–5 copies) are located at the other end of phage filament [13]. The best known application field of bacteriophages is phage display technology. With this method, one can identify short specific peptide sequences binding to surfaces [14], proteins [15] and even to human cells [16]. Recently, Lee et al. have developed high-power lithium ion battery electrodes by genetically modifying bacteriophage coat proteins to specifically bind SWNTs and $FePO_4$ [17].

Gold is a precious noble metal which has been utilized in everyday's life and in science since centuries. Colloidal gold nanoparticles (AuNPs) were first used in 4–5th centuries B.C. in ancient Egypt and China [18]. AuNPs are used in bioimaging [19], cancer therapy [20] and in electronic device fabrication [21] studies. As an anti-cancer agent, AuNPs can be functionalized with specific antibodies targeting specific cancer cells [20]. EDC/NHS (N-ethyl-N′-(3-dimethylaminopropyl) carbodiimide/N-hydroxysuccinimide) chemistry is widely applied to induce the formation of covalent bonding between Au surfaces and side chain amino acids of peptides [22]. Thiol groups (R-SH) have the highest binding affinity to Au surfaces (~200 kJ/mol) [23]. Therefore thiol modified oligonucleotides are used to be coupled with either AuNPs or Au surfaces via Au—S linkage for applications such as nanostructure fabrication, biosensor or drug delivery studies [24]. Similarly, amino acids "cysteine (Cys-C) and methionine (Met-M)" carrying sulfur (S) containing functional groups can be linked with AuNPs. Honda et al. [25] have reported on Au—S bond formation in monolayered L-cysteine on Au surfaces. Kim et al. [26] have genetically modified the immunoglobulin Fc-binding B-domain of protein G to express two Cys residues at its C-terminus. Recombinant G protein retained its IgG binding activity and provided strong Au surface binding ability due to Au—S linkage. Souza et al. [43] have recently investigated the coupling of AuNPs with wild type fd-phages via electrostatic interactions for cell targeting applications. Authors

* Tel.: +49 681 9382 252; fax: +49 681 9382 240.
E-mail addresses: n.korkmaz@kist-europe.de, nuriye_korkmaz@yahoo.com

0927-7765/$ – see front matter © 2013 Elsevier B.V. All rights reserved.
http://dx.doi.org/10.1016/j.colsurfb.2013.07.063

demonstrated that fd-phage molecules can bind AuNPs and form a network structure at pH values below pI of the major coat protein p8.

In this study, wild type fd- and genetically modified MMM-phages are investigated in terms of their gold binding affinities. Gold binding potential of engineered and wild-type phages were compared here by means of Quartz crystal microbalance (QCM), UV–vis absorption spectroscopy, scanning electron microscopy (SEM) and energy dispersive X-ray spectroscopy (EDX) analyses. EDX analyses showed that phage assemblies were coated with either AuNPs or reduced Au clusters after metallization experiments conducted with different concentrations of AuNPs or $HAuCl_4$ precursor solutions. Enhancing material binding property of engineered phage molecules may be a promising tool for bottom-up configuration of nanoelectronic device compartments.

2. Materials and methods

2.1. Cloning and phage amplification

E. coli MC1061 (New England Biolabs) and *E. coli* K91BluKan (K91BK) cells were applied for plasmid and phage amplification. *E. coli* K91BK cells and fd-tet vector were kindly provided by Prof. Dr. Georg P Smith (University of Missouri, USA). MMM short amino acid sequence was displayed on the N-terminus of the major coat protein p8 as discussed previously [27]. For phage amplification, *E. coli* K91BK cells were first transformed with fd and p8MMM vectors by electroporation. LB agar plates supplemented with tetracycline (Roth) and kanamycin (Roth) were utilized for positive colony selection. Phage purification was carried out by PEG/NaCl precipitation method as described before [28]. Phage concentration in terms of colony forming units per milliliter (cfu/ml) was measured by phage tittering. *E. coli* K91BK cells were infected with different dilutions of purified phages at 37 °C for 30 min and overnight grown colonies on LB agar plates supplemented with tetracycline and kanamycin were counted per ml. Final phage suspensions were dialyzed against 1× PBS at 4 °C overnight and stored in the fridge.

2.2. Binding measurements

Phage binding onto the gold surface was first analyzed by QCM measurements performed with Qsense E1, Sweden, according to manufacturer's instructions. Gold coated quartz crystals were purchased from Qsense. After the sensor was mounted in the probe arm of the instrument, washing steps with MilliQ water and 1× PBS (filter sterilized) were performed until the frequency signal became steady. 1 ml fd- or MMM-phages (10^{10} cfu/ml in 1× PBS) were injected at a flow rate of 15 μl/min and the sensor was rinsed with MilliQ at the same flow rate. In order to investigate the effect of pH on Au binding affinity of phages on Au coated quartz sensors, 300 μl of phages (10^9 cfu/ml) in 1× PBS buffer at pH 5, 7 and 9 was injected to the system and the sensors were washed with the same buffer at the same flow rate. Frequency change was measured for 5 different overtone resonance frequencies (15, 25, 35, 45, 54 and 64 MHz) at room temperature. Data were analyzed by QTools software program and experiments were repeated 3–4 times.

AuNP binding on bacteriophages was then analyzed by electron microscopy and UV–vis spectroscopy measurements. Citrate stabilized AuNPs were purchased from Sigma (~20 nm diameter, $\sim 7.2 \times 10^{11}$ particles/ml). Different volumetric dilutions (DF1 = 1:1, DF2 = 1:3 and DF3 = 1:10 [AuNP:PBS]) of AuNPs were prepared in 200 μl of 1× PBS and mixed with fd- and MMM-phages at a final concentration of 10^{10} cfu/ml. Samples were incubated at room temperature (RT) for 2 h on a rolling drum (7 rpm) and 70 μl of each was analyzed by UV–vis spectroscopy. For investigating the influence of pH on AuNP binding, citrate stabilized AuNPs were diluted in 1× PBS (pH 5, 7 and 9) at a 1:10 ratio and mixed with phages at a final concentration of 10^9 cfu/ml. Experiments were performed in triplicates.

2.3. Metallization

100 μl of fd- and MMM-phage solutions (10^{10} cfu/ml) were prepared in 3 mM, 30 mM and 60 mM $HAuCl_4 \cdot 3H_2O$ (Sigma). Phage samples were first incubated at RT for 2 h on a rolling drum (7 rpm) in order to initiate the Au^{3+} binding on phage filaments. After 2 h of incubation, samples were prepared for SEM imaging before the reduction. Chemical reduction reaction was performed with $NaBH_4$ (Sigma) at a final concentration of 15 mM and SEM samples were prepared as described below.

2.4. Microscopy

SEM imaging was conducted with an FEI Quanta 250 FEG scanning electron microscope at either 5 or 30 kV in high vacuum. EDAX™ Team EDX system was applied for the elemental characterization of phage assemblies. Industrial scale standard Si wafers with a native oxide layer was used for microscopy sample preparation. SiO_2 wafers were cleaned by sonication for 15 min in acetone, ethanol and finally in sterile MilliQ water. 10–20 μl was dropped on a piece of cleaned wafer. After 15–25 min, excess solution was removed with tissue paper, and 10–20 μl of sterile MilliQ water was dropped. After 5–10 min, the excess was removed and the wafers were blow-dried by nitrogen gas.

3. Results and discussion

3.1. Phage–Au surface binding

Introducing thiol groups to noble metal surfaces is a well-known method to induce metal-peptide conjugation [23]. Recently, our research group has generated a genetically engineered fd-phage construct carrying an MMM short amino acid sequence bearing three sulfur residues at N-terminal region of major coat protein p8 subunits (Fig. 1a). MMM-phages were shown to be conjugated with the enzyme glucose oxidase and applied as a biosensor [27]. Here, binding affinity of MMM-phages to Au surfaces and AuNPs is studied (Fig. 1b). Au—S bonding is commonly utilized in various application fields ranging from electronics to biosensor studies [29]. Thiolated oligonucleotide molecules are used for covalent binding to Au surfaces or NPs [24]. Recently, Kim et al. [26] have expressed two Cys residues at C-terminus of immunoglobulin Fc-binding B-domain of protein G. Recombinant G protein preserved its IgG binding activity and provided strong Au surface binding affinity due to Au—S linkage. Similarly, in this study genetically modified MMM-phages showed a considerable affinity to Au sensor. QCM analyses conducted with Au coated quartz crystal sensors showed an initial frequency decrease of ~160 Hz upon the injection of MMM-phages (Fig. 1d). At the end of washing step, net frequency change was measured as ~70 Hz showing that weakly or partially bound phage particles were removed from the Au sensor. As the frequency decrease is correlated with increase of mass accumulated on the QCM crystal [30], final frequency decrease demonstrates phage binding on the Au coated sensor surface. QCM result implies that MMM-phages bind the Au surface due to the interaction of MMM short amino acid sequence displayed on body part of the phage with the surface. Upon fd-phage injection on the other hand, frequency first decreased showing a mass accumulation on Au sensor and then increased after the washing step with 1× PBS revealing that fd-phages did not bind the Au surface (Fig. 1c).

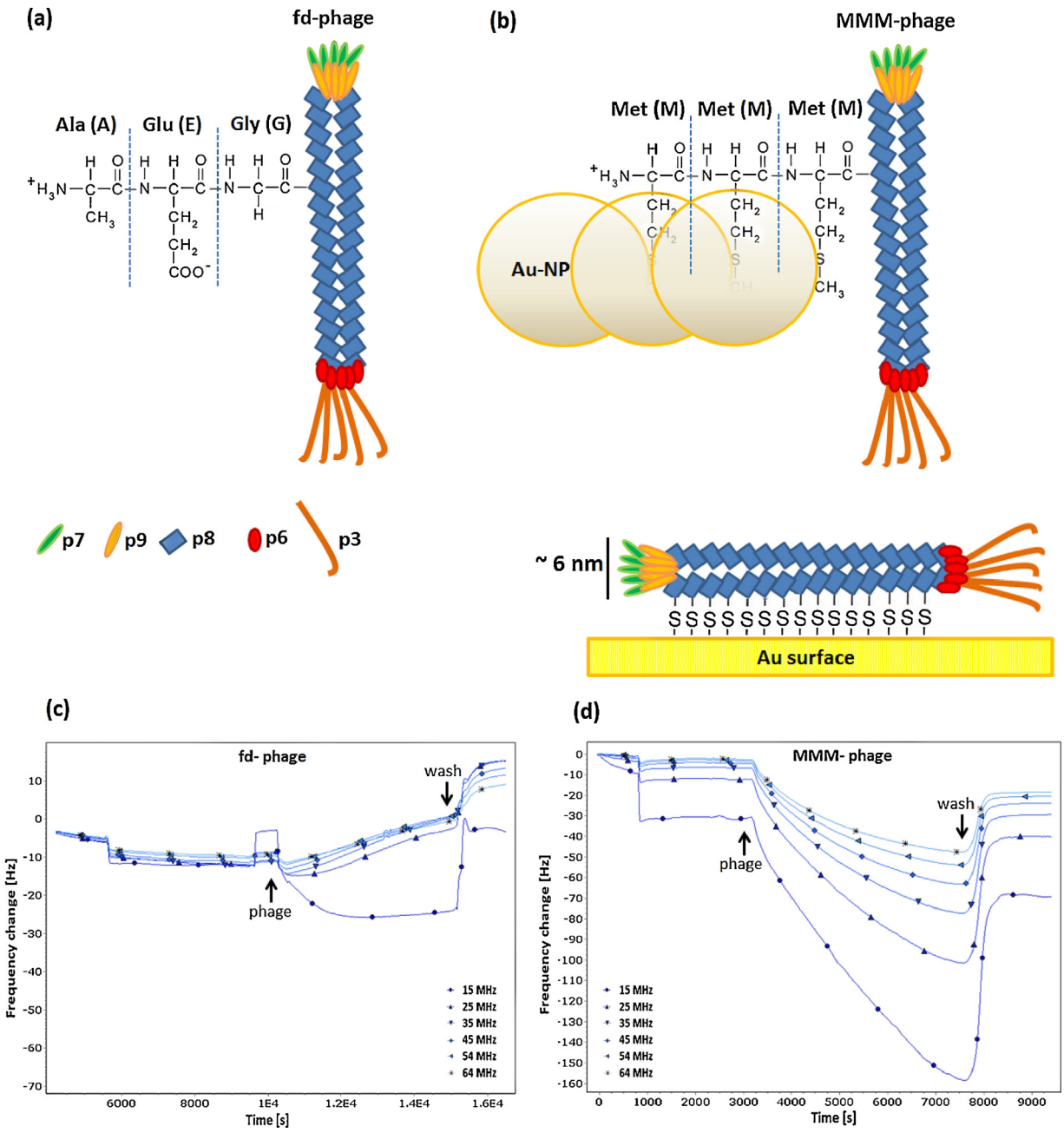

Fig. 1. Schematic representation of wild type fd- and MMM-phages. (a) fd-Phage filaments are composed of major coat protein p8 (2700–3000 copies) and minor coat proteins p3, p6, p7 and p9 (3–5 copies). MMM residues carrying sulfur (S) containing functional groups are displayed at N-terminus of main coat protein p8 subunits in order to obtain MMM-phages (b). MMM-phages are expected to bind AuNPs or Au surfaces via Au—S linkage. QCM analyses conducted with Au coated quartz crystal sensors showed no significant binding for fd-phages (c) and an observable frequency decrease (mass accumulation) for MMM-phages (d) after the final wash step (operating frequency overtones = 15–64 MHz).

3.2. AuNP conjugation to bacteriophages

In order to test the binding of AuNPs on bacteriophages, citrate stabilized NPs were first incubated with fd- and MMM-phages at a final concentration of 10^{10} cfu/ml. ~20 nm AuNPs are demonstrated in Fig. 2a. Okada et al. [31] have recently published a new protein purification system applying gold magnetic beads and a tandem Met tag. They showed that Met tagged EGFP was efficiently purified by magnetic beads based on Au—S linkage pointing at the binding affinity of Met molecules to Au particles. Similarly, upon incubation of colloidal AuNPs with MMM-phages, bacteriophages were observed to be decorated with AuNPs (Fig. 2b). Elemental analyses conducted by EDX confirmed the presence of Au on phage filaments. As fd-phages are incubated with colloidal AuNPs, in line with QCM analyses no evidence for strong Au-phage binding was found. Phage filaments were imaged as single dispersed filaments and AuNPs were mostly spread on the wafer (Fig. 2c).

Next, AuNP-phage binding was investigated at different dilutions of AuNPs prepared in 1× PBS buffer. As the dilution factor (DF) was increased, number of AuNPs attached on MMM-phage filaments decreased as expected (Fig. 2 – 2nd row). Moreover, phage filaments became more dispersed as AuNP concentration was decreased. Au peaks were detected by EDX measurements (Fig. 2 – 3rd row). Only a few AuNPs were detected on fd-phage agglomerates at DF1 (Fig. 2 – 4th row). Most probably, upon incubation of fd-phage solution on SiO_2 wafer, due to the drying

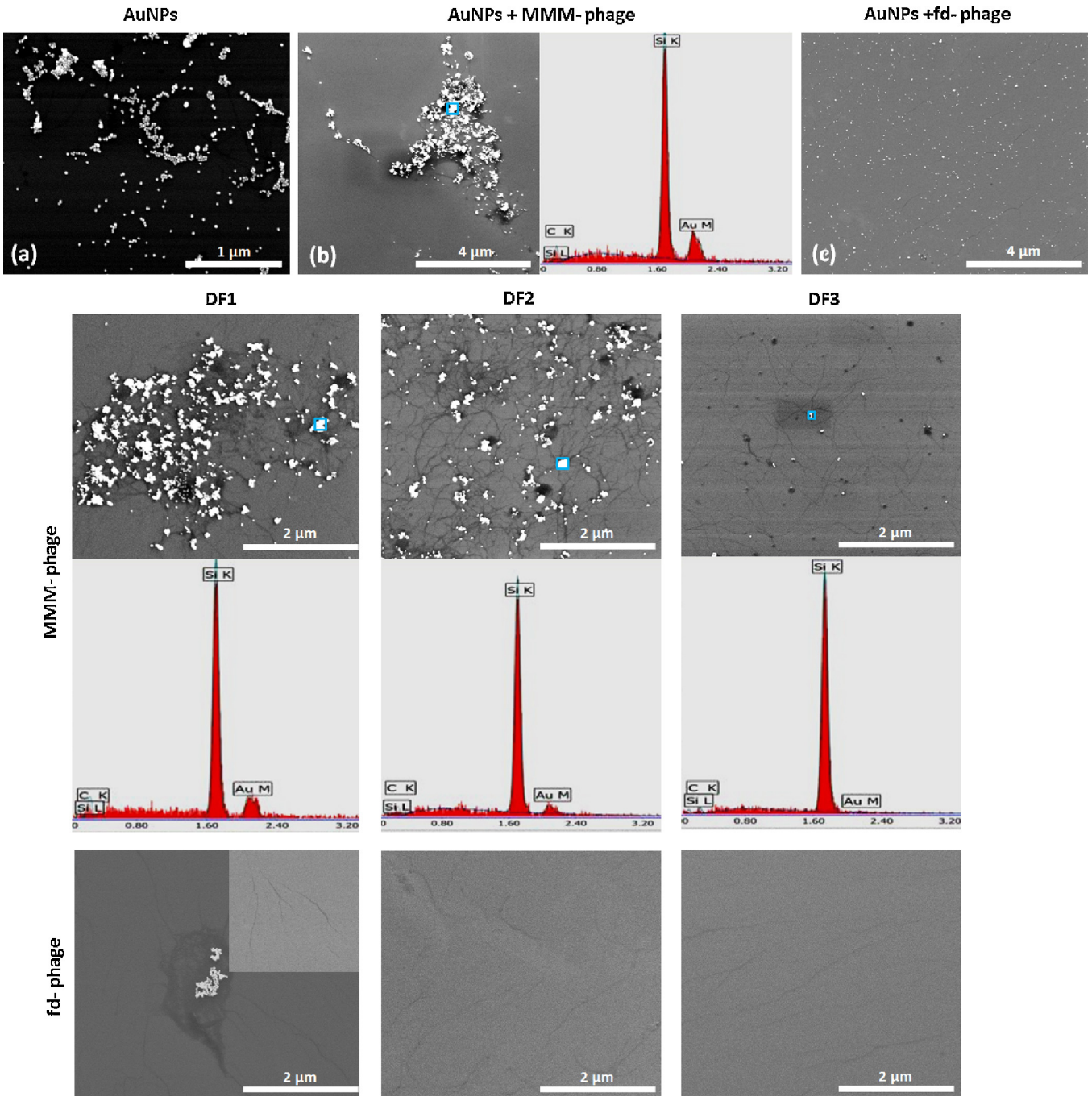

Fig. 2. SEM images of fd- and MMM-phages (10^{10} cfu/ml) incubated with either citrate stabilized AuNPs or with AuNPs diluted in 1× PBS. First row: Citrate stabilized AuNPs without any phage, with MMM-phages and with fd-phages. Second row: MMM-phages mixed with AuNPs diluted at 1:1 (DF1), 1:3 (DF2) and 1:10 (DF3) mixing ratios in 1× PBS buffer respectively. Third row: fd-phages mixed with AuNPs diluted at 1:1 (DF1), 1:3 (DF2) and 1:10 (DF3) in 1× PBS buffer. Pictures were taken at 30 kV. EDX analyses were conducted inside the blue boxes. (For interpretation of the references to color in this figure legend, the reader is referred to the web version of this article.)

process, phage filaments were aggregated randomly trapping some of AuNPs inside. For elongated fd-filaments no AuNP attachment was detected (Fig. 2 – 4th row, inset). Besides, at DF2 and DF3 no AuNP binding was observed for fd-phages (Fig. 2 – 4th row).

AuNP/phage binding was next investigated by UV–vis absorption spectroscopy. Spectral graphs are seen in Fig. 3. After citrate stabilized NPs were incubated with fd- and MMM-phages at a final concentration of 10^{10} cfu/ml, 70 µl of solutions with/without phages were analyzed. Colloidal AuNPs alone (red dashed lines) exhibited an absorption peak at 523 nm (Fig. 3a and c). Rayavarapu et al. have reported on antibody conjugation of citrate stabilized AuNPs where they observed a 5 nm peak shift after the conjugation by UV–vis spectroscopy [32]. In line with these findings, as MMM-phage particles were mixed with citrate stabilized AuNPs, a peak shift of 4 nm was detected showing the complex formation (Fig. 3c). For fd-phage case no peak shift thus no conjugation took place (Fig. 3d). Citrate containing buffers are commonly used to disperse and stabilize AuNPs by repulsive electrostatic forces. AuNPs tend to aggregate due to dipole interactions caused by shielded electric field as the ionic strength of environment increases [23]. Takada et al. [33] have recently conjugated AuNPs with DNA molecules via a photo triggered reaction. They reported that DNA conjugated

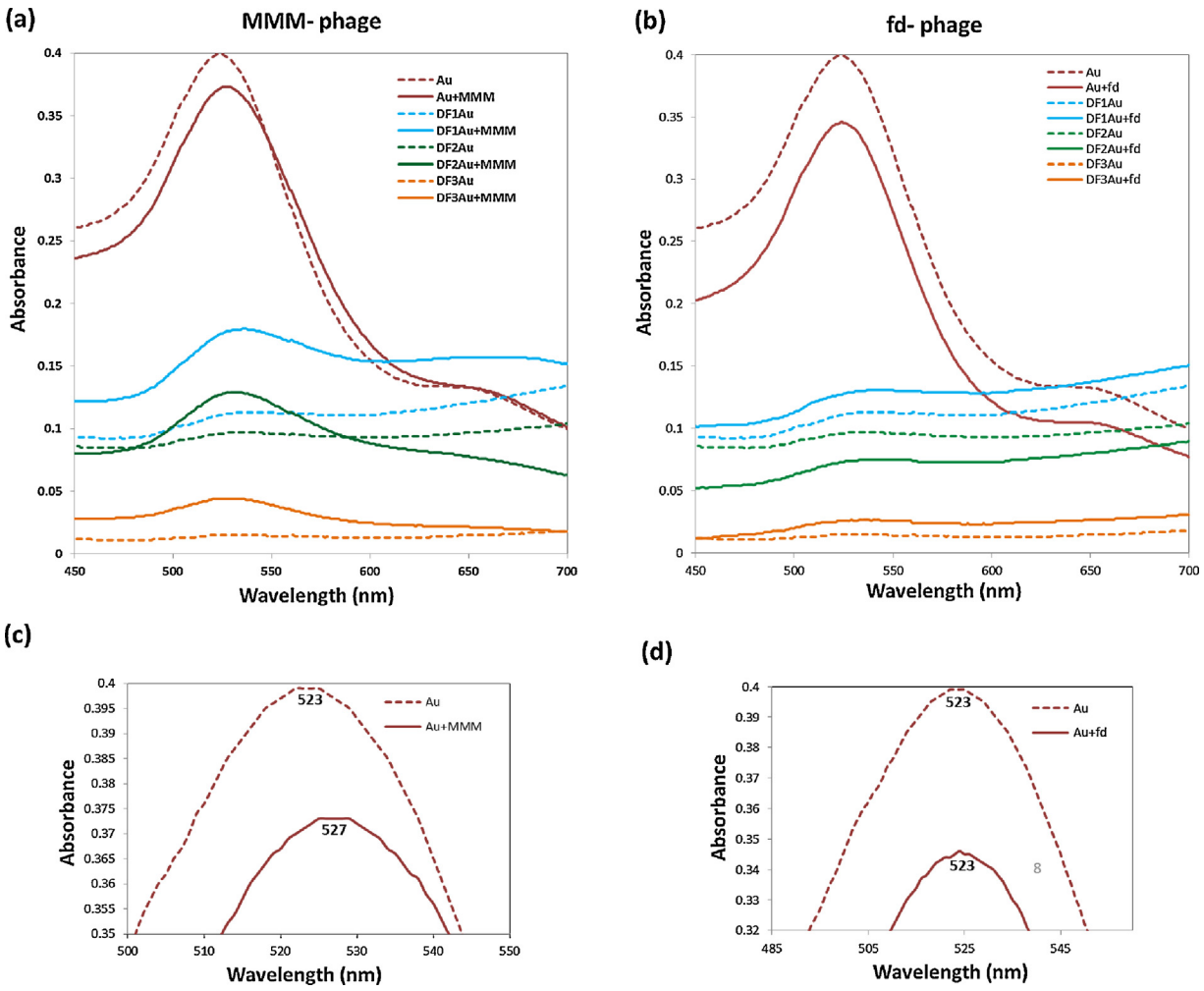

Fig. 3. UV/vis spectra of AuNP solutions mixed with MMM- (a) and fd-phages (b). Red curves represent undiluted citrate stabilized AuNPs. Diluted AuNPs were prepared in 1× PBS buffer at 1:1 (DF1), 1:3 (DF2) and 1:10 (DF3) mixing ratios. Final phage concentration was 10^{10} cfu/ml. Solid and dashed lines show absorbance spectra of AuNP solutions with and without phages respectively. (For interpretation of the references to color in this figure legend, the reader is referred to the web version of this article.)

AuNPs did not aggregate and remained stable giving a clear plasmon peak although unconjugated NPs did not show any peak. Similarly, when NPs were diluted in PBS buffer, they got aggregated and no distinct peak was observed (Fig. 3a and b – dashed lines). As MMM-phages were added at a final concentration of 10^{10} cfu/ml, aggregation was reduced due to the phage binding giving a more distinguishable plasmon peak at all DFs (Fig. 3a – solid lines). In contrast, fd-phage addition did not show any absorption peak implying that NPs did not attach to phage filaments and remain aggregated as before the phage addition (Fig. 3b).

3.3. *Effect of pH on gold binding affinity of phages*

Effect of pH on gold binding responses of wild type and engineered phages were first investigated by QCM analyses on Au sensors. Fig. 4a shows the binding responses of MMM- and fd-phages on Au surface at pH 5, 7 and 9. Injection of MMM-phages (10^9 cfu/ml) caused an overall frequency decrease of 12.1 ± 0.4, 10.1 ± 0.3 and 5.8 ± 1.7 Hz in 1× PBS at pH 5, 7 and 9 correspondingly (Fig. 4b). At pH 5 and pH 7, net frequency change was calculated to be approximately same (a deviation of 2 Hz) irrespective of the pH change. On the contrary, at pH 9 a relatively low frequency decrease of 5.8 ± 1.7 Hz was observed showing the hindrance of MMM-phage adsorption on the Au sensor. Net resonant frequency shifts upon injection of fd-phages (10^9 cfu/ml) were calculated to be 4.0 ± 1.1, 3.3 ± 0.3 and 3.8 ± 0.6 at pH 5, 7 and pH 9 respectively (Fig. 4b). These comparatively low frequency changes imply that fd-phages were not adsorbed efficiently on the Au sensor regardless of pH. Since bare gold is highly inert and cannot be oxidized unlike silver, in order to adsorb target peptide molecules or self-assembling monolayers (SAMs), no complicated modification of surface oxide layer is needed [34]. Metal–sulfur interaction is predominantly applied to link proteins on Au surfaces since Au—S bond is one of the strongest covalent bonds ($\Delta H^\circ \approx -45$ kcal/mol) [35]. Wild-type fd-phage does not carry any sulfur bearing amino acid residue on its major coat protein p8 subunits. Lack of sulfur functional groups most probably prevents fd-phages to bind strongly on bare Au electrodes. Electrostatic interactions can be neglected due to the inertness of Au sensor surface. Mendes et al. [36] have recently investigated the electron transfer of hexacyanoferrate (II/III) at gold surfaces coated with SAMs. Electrochemical impedence spectroscopy results showed different electron transfer responses at different pH values (pH 4–8) [36]. However, no charge transfer resistance change of bare Au electrode was observed upon the pH change. Additionally, SAM immobilization on Au sensor was not reported to be affected by the pH shift from pH 4 to pH 8. Likewise, engineered MMM-phages showed similar binding responses at pH 5 and pH 7 (Fig. 4a) which was also observed by Johnson and Mutharasan [35] for G-protein coupling to Au surface at pH 3, 5 and 7.2.

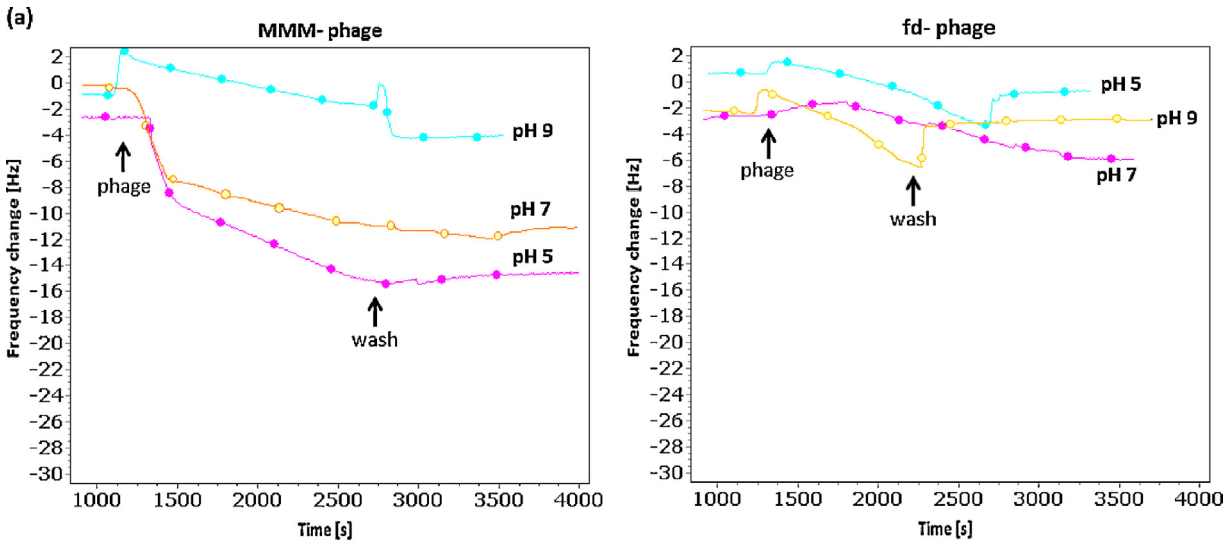

(b)

	Net resonant frequency decrease		
	pH 5	pH 7	pH 9
MMM- phage	12.1 ± 0.4 Hz	10.1 ± 0.3 Hz	5.8 ± 1.7 Hz
fd- phage	4.0 ± 1.1 Hz	3.3 ± 0.3 Hz	3.8 ± 0.6 Hz

Fig. 4. QCM adsorption analyses of fd- and MMM-phages (10^9 cfu/ml) on Au coated quartz crystal sensors at pH 5, pH 7 and pH 9 (a) and the list of calculated overall frequency changes at the 3rd frequency overtone ($n = 3$) (b).

Gold binding affinities at various pH conditions were next investigated with AuNPs. Citrate stabilized AuNPs (1:10 dilution) were incubated with fd- and MMM-phages (10^9 cfu/ml) at pH 5, 7 and 9. Fig. 5 shows the corresponding SEM images. Although MMM-phages showed an effective binding response to AuNPs at pH 5 and pH 7, Au binding was strongly impaired at pH 9. This can be explained by considering electrostatic interactions and stability of Au—S bonding. Khan et al. [37] have investigated the

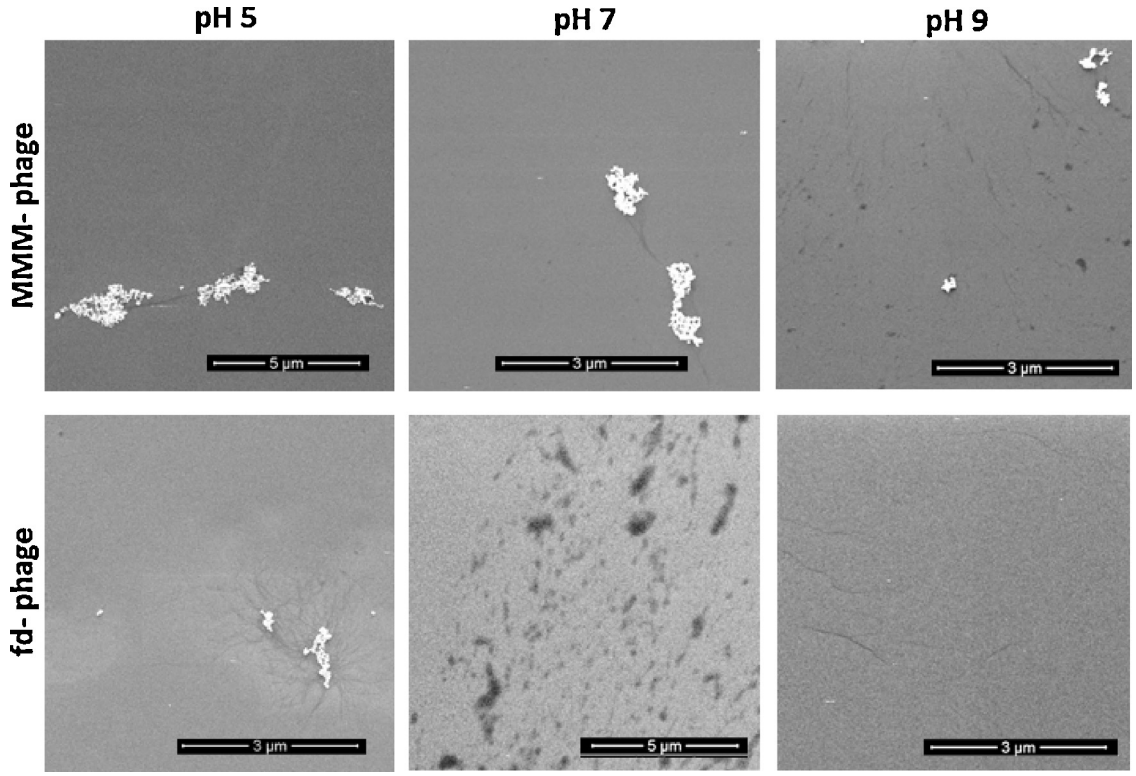

Fig. 5. SEM images of fd- and MMM-phages (10^9 cfu/ml) incubated with citrate stabilized AuNPs at pH 5, 7 and 9. Pictures were taken at 30 kV.

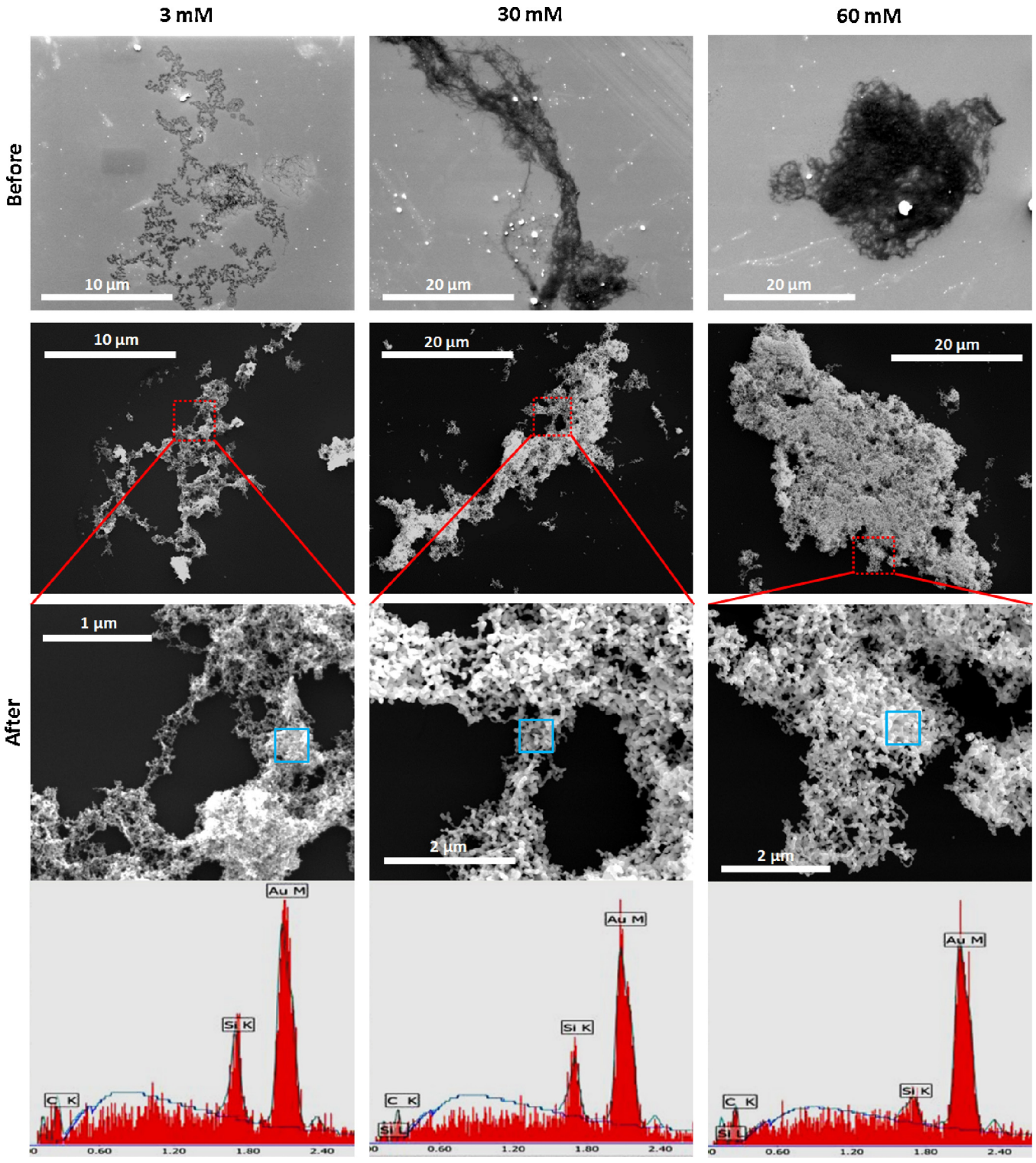

Fig. 6. SEM images of fd-phages treated with various concentrations of $HAuCl_4$ precursor solutions (3 mM, 30 mM and 60 mM) before and after chemical reduction reaction. SEM pictures before and after reduction were taken at 5 kV and 30 kV respectively. EDX analyses were conducted inside the blue boxes. (For interpretation of the references to color in this figure legend, the reader is referred to the web version of this article.)

electrostatic binding of AuNPs to TMVs. Citrate stabilized AuNPs were shown to be negatively charged at a broad pH range (pH 3–8). Below the isoelectric point (pI) of 3.5, TMVs were shown to be decorated with AuNPs due to electrostatic interactions. Theoretical pI values of mature form (without signal peptide) of major coat protein p8 of MMM- and fd-phages were calculated as 6.28 and 8.25 respectively. At pH 9, MMM-phages should be negatively charged repelling the AuNPs (Fig. 5 – 1st row). Moreover, Bhatt et al. [29] have already reported on instability of Au—S bonds at elevated pHs like pH 9 which would also hinder the AuNP attachment. At pH 7 and pH 9, fd-phages are expected to carry a net negative surface charge which prevents them to bind negatively charged AuNPs as seen in Fig. 5 – 2nd row. However, they should be protonated at pH 5 (pI < 6.28) to carry more positive charges

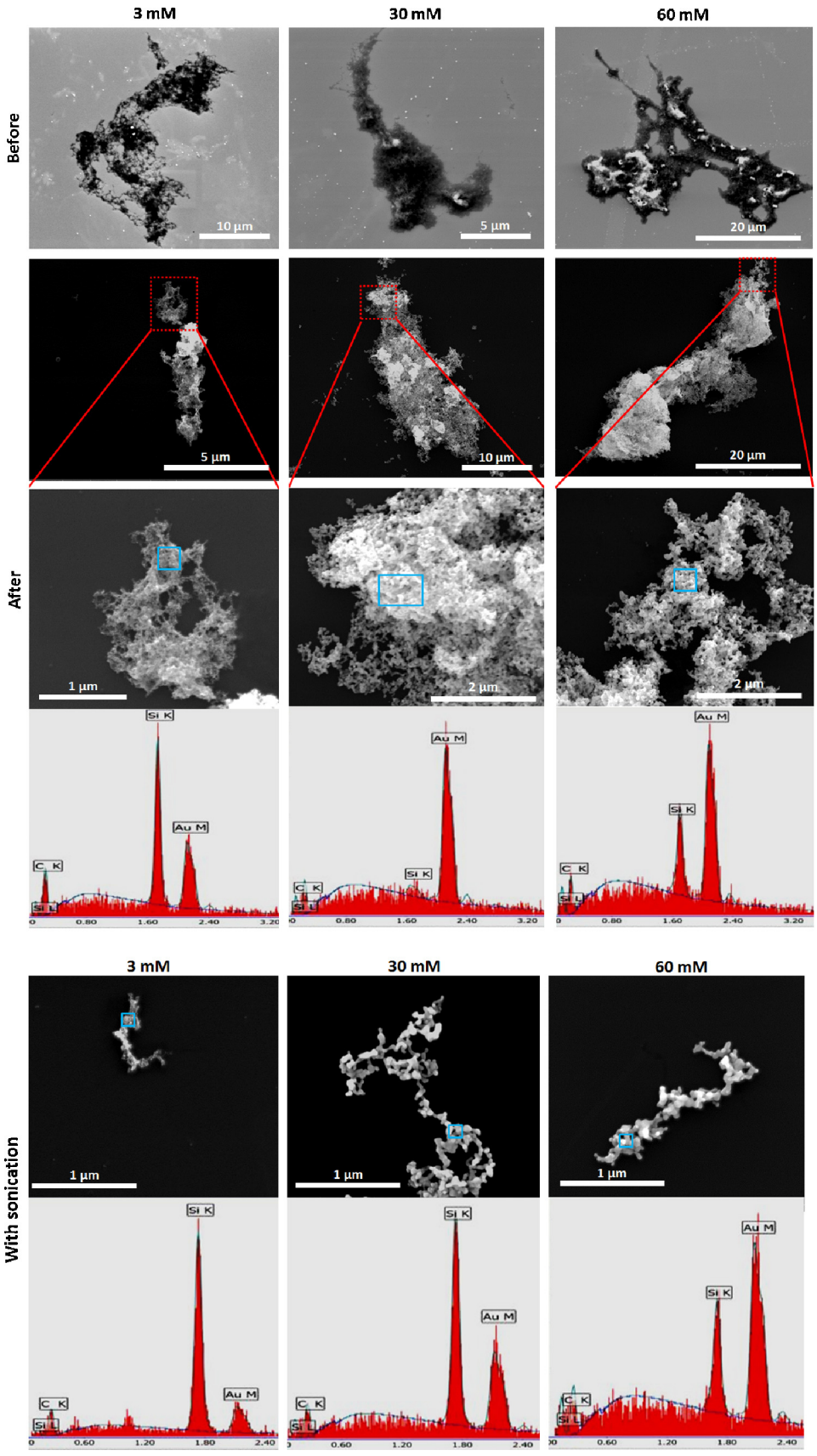

Fig. 7. SEM images of MMM-phages treated with various concentrations of $HAuCl_4$ precursor solutions (3 mM, 30 mM and 60 mM) before and after chemical reduction reaction. Last row: Metallized MMM- phages after sonication. SEM pictures before and after reduction were taken at 5 kV and 30 kV respectively. EDX analyses were conducted inside the blue boxes. (For interpretation of the references to color in this figure legend, the reader is referred to the web version of this article.)

promoting AuNP binding. This outcome is supported by Souza et al. [43] who investigated the electrostatic interaction of fd-phages with citrate stabilized AuNPs at various pHs. They reported that wild type phages could bind AuNPs at pH values lower than the pI of major coat protein p8 due to the electrostatic attraction which is in line with the results presented in this study.

3.4. Metallization

After showing that MMM-phages have remarkable binding affinity to Au surface by means of QCM, SEM and UV–vis spectroscopy analyses, metallization potential of fd- and MMM-phages were investigated upon chemical reduction reaction. As it was shown before for bio-templates such as DNA, RNA, microtubules or TMV particles, it is possible to deposit metallic particles on biological molecules with reducing agents. Decoration of bio-templates with metal clusters after chemical reduction is presumed to take place in three stages: (1) metal ion attachment at amino acids like histidine or cysteine, (2) metal ion (M^+) reduction to metallic M(0) upon reducing agent treatment and (3) formation of metal clusters after a critical M(0) concentration was obtained [3]. Since it is known that fd-phage has a net negative surface charge density at physiological conditions [38], it is expected that they bind Au^{3+} ions upon incubation with $HAuCl_4$ precursor solution. As seen in Fig. 6, fd-phages formed bundle like structures as they were mixed with 3 mM, 30 mM and 60 mM $HAuCl_4$ salt solutions. As the precursor concentration was increased, level of bundling got increased by inducing attractive forces between phage filaments as can be explained by the Manning's theory of counterion condensation [39]. Increase in bundling efficiency by increased concentration of divalent ions was already shown for actin filaments by Yu and Carlsson's bundling model [40]. Similarly, we have recently shown that phage bundling is enhanced by increasing Co^{2+} and Ca^{2+} concentrations [41]. As fd- and MMM-phage bundling is compared, it is seen that MMM-phages formed more condensed and more intertwined structures at the same Au precursor concentration. This implies that MMM-phages bound more Au^{3+} ions with a higher affinity than fd-phages due to the presence of displayed Met amino acids. Upon the addition of $NaBH_4$ solution which is a strong reducing agent [42], bound Au^{3+} ions were reduced. Corresponding SEM images demonstrated the deposited Au clusters on bacteriophage bundles (Figs. 6 and 7). EDX spectra can be seen in zoomed-in images showing the Au and C signals originated from deposited Au particles and bacteriophage filaments respectively. After sonicating the metallized MMM-samples, larger aggregates were separated and smaller filamentous structures around 1–2 μm long were observed (Fig. 7 – last row).

4. Conclusion

In this study, gold binding affinity of genetically engineered filamentous MMM-bacteriophages was investigated by QCM, UV–vis spectrophotometry and SEM analyses. QCM measurements demonstrated that MMM short amino acid sequence displayed on major coat protein p8 enables attachment of recombinant phages to Au surfaces via Au—S linkage. UV–vis absorption measurements revealed MMM-phage conjugation to AuNPs and showed the stabilizing effect of recombinant phage attachment on aggregation of AuNPs. SEM analyses showed AuNPs located on MMM-phage filaments. Binding response of MMM-phages on Au coated quartz sensors was similar at pH 5 and pH 7 and as the buffer pH was increased to pH 9, phage adsorption was hindered. Although wild type fd-phages did not show a significant binding response to bare Au electrode at various pHs, due to the electrostatic interactions between citrate stabilized AuNPs and fd-phage molecules at pH 5, NPs were observed to attach fd-phage molecules. Bacteriophages formed bundle like structures as they were incubated with 3 mM, 30 mM and 60 mM $HAuCl_4$ salt solution. As the precursor concentration was increased, level of bundling got increased by inducing attractive forces between phage filaments caused by bound Au^{3+} ions. MMM-phages formed more condensed and more intertwined structures than fd-phages implying that MMM-phages bound more Au^{3+} ions due to the presence of displayed Met amino acids. Chemical reduction of bound Au^{3+} ions with $NaBH_4$ at different $HAuCl_4$ precursor concentrations resulted in metallized phage filament formation. EDX measurements confirmed the presence of Au particles on both AuNP decorated and electroless metallized phage structures. Further investigations on patterning and controlled immobilization of genetically modified bacteriophages may contribute to bio-templated nanowire development studies or biosensor applications.

Acknowledgment

This work was supported by Korea Institute of Science and Technology-Europe basic research program.

References

[1] D. Mijatovic, J.C. Eijkel, A. van den Berg, Technologies for nanofluidic systems: top-down versus bottom-up – a review, Lab Chip 5 (2005) 492–500.
[2] J.M. Slocik, S.N. Kim, T.A. Whitehead, D.S. Clark, R.R. Naik, Biotemplated metal nanowires using hyperthermophilic protein filaments, Small 5 (2009) 2038–2042.
[3] Y. Yang, B.H. Constance, P.A. Deymier, J. Hoying, S. Raghavan, J.J. Zelinski, Electroless metal plating of microtubules: effect of microtubule-associated proteins, J. Mater. Sci. 39 (2004) 1927–1933.
[4] C. Erler, K. Günther, M. Mertig, Photo-induced synthesis of DNA-templated metallic nanowires and their integration into micro-fabricated contact arrays, Appl. Surf. Sci. 255 (2009) 9647–9651.
[5] E. Dujardin, C. Peet, G. Stubbs, J.N. Culver, S. Mann, Organization of metallic nanoparticles using tobacco mosaic virus templates, Nano Lett. 3 (2003) 413–417.
[6] N. Korkmaz, F. Börrnert, D. Köhler, R.G. Mendes, A. Bachmatiuk, M.H. Rümmeli, B. Büchner, L.M. Eng, G. Rödel, Nanotechnology 22 (2011) 375606.
[7] Q. Gu, C. Cheng, D.T. Haynie, Cobalt metallization of DNA: toward magnetic nanowires, Nanotechnology 16 (2005) 1358–1363.
[8] Y. Wang, G. Ouyang, J. Zhang, Z. Wang, A DNA-templated catalyst: the preparation of metal-DNA nanohybrids and their application in organic reactions, Chem. Commun. (Camb.) 46 (2010) 7912–7914.
[9] T. Ohmichi, Y. Kawamoto, P. Wu, D. Miyoshi, H. Karimata, N. Sugimoto, DNA-based biosensor for monitoring pH in vitro and in living cells, Biochemistry 44 (2005) 7125–7130.
[10] F. Wang, B. Cao, C. Mao, Bacteriophage bundles with pre-aligned Ca initiate the oriented nucleation and growth of hydroxylapatite, Chem. Mater. 22 (2010) 3630–3636.
[11] O. Morag, G. Abramov, A. Goldbourt, Similarities and differences within members of the Ff family of filamentous bacteriophage viruses, J. Phys. Chem. B 115 (2011) 15370–15379.
[12] Y.A. Wang, X. Yu, S. Overman, M. Tsuboi, G.J. Thomas Jr., E.M. Egelman, The structure of a filamentous bacteriophage, J. Mol. Biol. 361 (2006) 209–215.
[13] H.B. Lowman, Bacteriophage display and discovery of peptide leads for drug development, Annu. Rev. Biophys. Biomol. Struct. 26 (1997) 401–424.
[14] S.R. Whaley, D.S. English, E.L. Hu, P.F. Barbara, A.M. Belcher, Selection of peptides with semiconductor binding specificity for directed nanocrystal assembly, Nature 405 (2000) 665–668.
[15] I. López, M.A. Pardo, A phage display system for the identification of novel Anisakis simplex antigens, J. Immunol. Methods 373 (2011) 247–251.
[16] M. Whitney, J.L. Crisp, E.S. Olson, T.A. Aguilera, L.A. Gross, L.G. Ellies, R.Y. Tsien, Parallel in vivo and in vitro selection using phage display identifies protease-dependent tumor-targeting peptides, J. Biol. Chem. 285 (2010) 22532–22541.
[17] Y.J. Lee, H. Yi, W.J. Kim, K. Kang, D.S. Yun, M.S. Strano, G. Ceder, A.M. Belcher, Fabricating genetically engineered high-power lithium-ion batteries using multiple virus genes, Science 324 (2009) 1051–1055.
[18] A. Moores, F. Goettmann, The plasmon band in noble metal nanoparticles: an introduction to theory and applications, New J. Chem. 30 (2006) 1121–1132.
[19] E. Hutter, D. Maysinger, Gold nanoparticles and quantum dots for bioimaging, Microsc. Res. Tech. 74 (2011) 592–604.
[20] A. Kumar, H. Ma, X. Zhang, K. Huang, S. Jin, J. Liu, T. Wei, W. Cao, G. Zou, X.J. Liang, Gold nanoparticles functionalized with therapeutic and targeted peptides for cancer treatment, Biomaterials 33 (2012) 1180–1189.

[21] T. Ogawa, K. Kobayashi, G. Masuda, T. Takase, S. Maeda, Electronic conductive characteristics of devices fabricated with 1,10-decanedithiol and gold nanoparticles between 1-μm electrode gaps, Thin Solid Films 393 (2001) 374–378.
[22] D. Li, Q. He, Y. Cui, L. Duan, J. Li, Immobilization of glucose oxidase onto gold nanoparticles with enhanced thermostability, Biochem. Biophys. Res. Commun. 355 (2007) 488–493.
[23] R.A. Sperling, W.J. Parak, Surface modification, functionalization and bioconjugation of colloidal inorganic nanoparticles, Philos. Trans. A: Math. Phys. Eng. Sci. 368 (2010) 1333–1383.
[24] F. Tielens, E. Santos, AuS and SH bond formation/breaking during the formation of alkanethiol SAMs on Au(1 1 1): a theoretical study, J. Phys. Chem. C 114 (2010) 9444–9452.
[25] M. Honda, y. Baba, N. Hirao, T. Sekiguchi, Metal–molecular interface of sulfur-containing amino acid and thiophene on gold surface, J. Phys.: Conf. Ser. (2008), http://dx.doi.org/10.1088/1742-6596/100/5/052071.
[26] H. Kim, D.Y. Kang, H.J. Goh, B.K. Oh, R.P. Singh, S.M. Oh, J.W. Choi, Analysis of direct immobilized recombinant protein G on a gold surface, Ultramicroscopy 108 (2008) 1152–1156.
[27] Y.R. Kang, K.H. Hwang, J.H. Kim, C.H. Nam, S.W. Kim, Disposable amperometric biosensor based on nanostructured bacteriophages for glucose detection, Meas. Sci. Technol. 21 (2010) 105804, http://dx.doi.org/10.1088/0957-0233/21/10/105804.
[28] D.Y. Jeon, K.H. Hwang, S.J. Park, Y.J. Kim, M.K. Joo, S.E. Ahn, G.T. Kim, C.H. Nam, Controlled surface adsorption of fd filamentous phage by tuning of the pH and the functionalization of the surface, J. Appl. Phys. 109 (2011) 064701, http://dx.doi.org/10.1063/1.3549113.
[29] N. Bhatt, P.J. Huang, N. Dave, J. Liu, Dissociation and degradation of thiol-modified DNA on gold nanoparticles in aqueous and organic solvents, Langmuir 27 (2011) 6132–6137.
[30] E. Uttenthaler, M. Schräml, J. Mandel, S. Drost, Ultrasensitive quartz crystal microbalance sensors for detection of M13-phages in liquids, Biosens. Bioelectron. 16 (2001) 735–743.
[31] Y. Okada, T.Y. Takano, N. Kobayashi, A. Hayashi, M. Yonekura, Y. Nishiyama, T. Abe, T. Yoshida, T.A. Yamamoto, S. Seino, T. Doi, New protein purification system using gold-magnetic beads and a novel peptide tag, the methionine tag, Bioconjug. Chem. 22 (2011) 887–893.
[32] R.G. Rayavarapu, W. Petersen, C. Ungureanu, J.N. Post, T.G. van Leeuwen, S. Manohar, Synthesis and bioconjugation of gold nanoparticles as potential molecular probes for light-based imaging techniques, Int. J. Biomed. Imag. 2007 (2007) 29817.
[33] T. Takada, Y. Kawano, M. Nakamura, K. Yamana, Photo-triggered generation of a free thiol group on DNA: application to DNA conjugation, Tetrahedron Lett. 53 (2012) 78–81.
[34] J.C. Love, L.A. Estroff, J.K. Kriebel, R.G. Nuzzo, G.M. Whitesides, Self-assembled monolayers of thiolates on metals as a form of nanotechnology, Chem. Rev. 105 (2005) 1103–1169.
[35] B.N. Johnson, R. Mutharasan, pH effect on protein G orientation on gold surfaces and characterization of adsorption thermodynamics, Langmuir 28 (2012) 6928–6934.
[36] R.K. Mendes, R.S. Freire, C.P. Fonseca, S. Neves, L.T. Kubota, Characterization of self-assembled thiols monolayers on gold surface by electrochemical impedance spectroscopy, J. Braz. Chem. Soc. 15 (2004) 849–855.
[37] A.A. Khan, E.K. Fox, M.Ł. Górzny, E. Nikulina, D.F. Brougham, C. Wege, A.M. Bittner, pH control of the electrostatic binding of gold and iron oxide nanoparticles to tobacco mosaic virus, Langmuir 29 (2013) 2094–2098.
[38] J.X. Tang, P.A. Janmey, The polyelectrolyte nature of F-actin and the mechanism of actin bundle formation, J. Biol. Chem. 271 (1996) 8556–8563.
[39] G.S. Manning, The molecular theory of polyelectrolyte solutions with applications to the electrostatic properties of polynucleotides, Q. Rev. Biophys. 2 (1978) 179–246.
[40] X. Yu, A.E. Carlsson, Multiscale study of counterion-induced attraction and bundle formation of F-actin using an Ising-like mean-field model, Biophys. J. 85 (2003) 3532–3543.
[41] N. Korkmaz, Y.J. Kim, C.H. Nam, Bacteriophages as templates for manufacturing supramolecular structures, Macromol. Biosci. 13 (2013) 376–387.
[42] K.C. Song, S.M. Lee, T.S. Park, B.S. Lee, Preparation of colloidal silver nanoparticles by chemical reduction method, Korean J. Chem. Eng. 26 (2004) 153–155.
[43] G.R. Souza, D.R. Christianson, F.I. Staquicini, M.G. Ozawa, E.Y. Snyder, R.L. Sidman, J.H. Miller, W. Arap, R. Pasqualini, Networks of gold nanoparticles and bacteriophage as biological sensors and cell-targeting agents, Proc. Natl. Acad. Sci. 103 (2006) 1215–1220.